

Short Communication

## Nano- $\text{Li}_4\text{Ti}_5\text{O}_{12}$ Pore Microspheres: A High Power Electrode Material for Lithium Ion Batteries

Wei Fang<sup>1,2</sup>, Yulin Ma<sup>1</sup>, Pengjian Zuo<sup>1</sup>, Xinqun Cheng<sup>1</sup>, Geping Yin<sup>1,\*</sup>

<sup>1</sup> School of Chemical Engineering and Technology, Harbin Institute of Technology, No.92, West Da-Zhi Street, Harbin 150001 China

<sup>2</sup> School of Chemistry, Baicheng Normal University, No.9, zhongxing dongda road, Baicheng 137000 China

\*E-mail: [yingeping@hit.edu.cn](mailto:yingeping@hit.edu.cn)

Received: 1 December 2012 / Accepted: 2 January 2013 / Published: 1 February 2013

Nano- $\text{Li}_4\text{Ti}_5\text{O}_{12}$  pore microspheres were synthesized by hydrothermal and subsequent calcination methods using  $\text{Ti}(\text{OC}_4\text{H}_9)_4$  and  $\text{LiAc}\cdot 2\text{H}_2\text{O}$  as raw materials. TEM analysis highlights the excellent crystallinity of the nano-sized  $\text{Li}_4\text{Ti}_5\text{O}_{12}$  primary particles with the size between 30–40 nm. As anode material of lithium ion batteries, the nano- $\text{Li}_4\text{Ti}_5\text{O}_{12}$  exhibits higher capacity and better rate capability, delivering the 1 C capacity close to the theoretical value of  $175 \text{ mAh g}^{-1}$ , 10C capacity of  $133 \text{ mAh g}^{-1}$  and even 60 C capacity of  $80 \text{ mAh g}^{-1}$ . The ameliorated electrode-performance is ascribed to nanostructure of the material that provides shorter diffusion-paths and faster migration rate for both of ions and electrons..

**Keywords:** nano- $\text{Li}_4\text{Ti}_5\text{O}_{12}$ , pore microspheres, lithium ion battery, high rate

### 1. INTRODUCTION

In recent ten years of research, spinal  $\text{Li}_4\text{Ti}_5\text{O}_{12}$  has been regarded as a popular anode material due to the highly reversible lithium intercalation and deintercalation prosperities ( $\text{Li}_4\text{Ti}_5\text{O}_{12} + 3\text{Li}^+ + 3\text{e}^- \rightarrow \text{Li}_7\text{Ti}_5\text{O}_{12}$ ) [1-2]. It has a theoretical capacity of  $175 \text{ mAh g}^{-1}$  with a very flat charge/discharge potential plateau at 1.55 V due to the stable  $\text{Ti}^{4+}/\text{Ti}^{3+}$  redox couple versus and experiences zero-strain during lithium intercalation/deintercalation [3-6]. Furthermore,  $\text{Li}_4\text{Ti}_5\text{O}_{12}$  also saves other advantages such as superior safety, excellent structural stability, high rate capability, low toxicity, low raw material cost and long cycle life [7-8]. Hence,  $\text{Li}_4\text{Ti}_5\text{O}_{12}$  is an important candidate as anode material of future lithium ion battery.

However,  $\text{Li}_4\text{Ti}_5\text{O}_{12}$  has intrinsic disadvantages of low electronic conductivity ( $<10^{-13} \text{ S cm}^{-1}$ ), and slow lithium-ion diffusion ( $10^{-9}$ – $10^{-13} \text{ cm}^2 \text{ s}^{-1}$ ), which restrict its practical application in lithium-

ion batteries [9-13]. To enhance rate performance of  $\text{Li}_4\text{Ti}_5\text{O}_{12}$  anode materials, several methods have been investigated and reported, such as doping with metal cations (Mg, Sn, Ag, Cu or Al etc) [14-18], coating with carbon [19], modifying surface morphology with titanium nitride [20,21]. Moreover, carbon nanotubes, carbon nanofiber or graphene are incorporated with  $\text{Li}_4\text{Ti}_5\text{O}_{12}$  by mechanical mixing and nanotechnology have been proposed to overcome this obstacle [22-23]. Especially those materials on the nanometer level, increase the contact area with electrolyte and shorten the migrating path of Li ions during intercalation/extraction, which would lead to improved lithium intercalation kinetics, and result in a higher utilization and better rate properties [25-31]. For instance, nanosheets and nanowires synthesized by Yang et al and Wei et al exhibited high rate capability and superior cycling stability at high current densities [32,33]. In contrast, improving rate performance and maintaining the high tap density would significantly increase the volumetric energy density of  $\text{Li}_4\text{Ti}_5\text{O}_{12}$ . Depending on the material morphology and particle size, spherical  $\text{Li}_4\text{Ti}_5\text{O}_{12}$  material has higher tap density than irregular particles and improved safety associated with their low interfacial energy [21,34,35].

Here we described the synthesis of nano- $\text{Li}_4\text{Ti}_5\text{O}_{12}$  pore microspheres using a hydrothermal self-assembly wet chemistry route followed by short time heat treatment. The morphology of the prepared  $\text{Li}_4\text{Ti}_5\text{O}_{12}$  pore microspheres was characterized by means of SEM and TEM, and the electrochemical performance of the  $\text{Li}_4\text{Ti}_5\text{O}_{12}$  microspheres powders with nano-structured was further tested as an anode material for lithium ion battery, as an evidence for its competency for further utilization in lithium ion battery of high rate performance.

## 2. EXPERIMENTS

### 2.1. Synthesis of nano-structured $\text{Li}_4\text{Ti}_5\text{O}_{12}$ pore microspheres

The preparation of the nanostructured powder  $\text{Li}_4\text{Ti}_5\text{O}_{12}$  can be briefly described by the following process. Firstly, 2mL of tetrabutyl titanate (TTIP,  $\text{Ti}(\text{OC}_4\text{H}_9)_4$ , 99%, Aldrich) was dissolved in 20mL of absolute ethyl alcohol and 0.5g of lithium acetate ( $\text{C}_2\text{H}_3\text{O}_2\text{Li} \cdot 2\text{H}_2\text{O}$ , 99%, Aldrich) was dissolved in 20mL of absolute ethyl alcohol in beaker, respectively. Then, two mixtures were transferred to a sealed stainless steel Teflon-lined reaction vessel (60 mL) and 3 drops of distilled water was added to the mixed solution of TTIP and LiAc drop by drop. The autoclave was sealed and heated at 170°C for 3 days, and then cooled to room temperature naturally. The resultant powder was dried at 80°C for 24 h under vacuum to obtain the precursor of  $\text{Li}_4\text{Ti}_5\text{O}_{12}$ . The precursor was calcinated at 1050°C for 1 h with a heating rate of 5°C  $\text{min}^{-1}$  in a muffle furnace under air atmosphere and then cooled to room temperature naturally in the furnace.

### 2.2 Material characterization

Crystal structure of the powder was determined by X-ray powder diffraction (XRD, Rigaku D/max- $\gamma$ B) with a Cu anode as X-ray source ( $\lambda = 1.54059 \text{ \AA}$ ), at a scanning rate of 6°  $\text{min}^{-1}$  in range of

10–90°. The morphology of  $\text{Li}_4\text{Ti}_5\text{O}_{12}$  material was characterized by scanning electron microscope (SEM, Hitachi S-4800) and transmission electron microscope (TEM, Hitachi H-7650).

### 2.3 Electrochemical characterization

The electrode was prepared as follows: 80wt.%  $\text{Li}_4\text{Ti}_5\text{O}_{12}$  powder, 10wt.% carbon black, and 10wt.% polyvinylidene fluoride (PVDF) were dispersed in 1-methyl-2-pyrrolidinone (NMP) to prepare a slurry. The resultant slurry was then coated on a copper foil and dried at 120°C for 10 h in a vacuum oven. The thickness of  $\text{Li}_4\text{Ti}_5\text{O}_{12}$  anode was around 60  $\mu\text{m}$ . The work electrode was punched into circular discs. Electrochemical performance of the electrode was measured with 2025 type coin cell with lithium foil as the counter electrode and reference electrode, and Celgard2400 as the separator. The electrolyte was 1mol L<sup>-1</sup>  $\text{LiPF}_6$  dissolved in a 1:1:1 (vol.%) mixture of ethylene carbonate(EC), dimethyl carbonate (DMC) and ethyl methyl carbonate (EMC). The cells were assembled in an argon glove box where both moisture and oxygen content were less than 1ppm and were cycled between 1V and 2.5V versus  $\text{Li/Li}^+$  at 1-60 C rates (1 C = 175 mAh g<sup>-1</sup>).

## 3. RESULTS AND DISCUSSION

Fig.1 shows the XRD patterns of the  $\text{Li}_4\text{Ti}_5\text{O}_{12}$ . The diffraction peaks are indexed at  $2\theta = 18.4, 35.6, 37.1, 43.3, 47.4, 57.2, 62.8$  and  $66.1^\circ$ , indicating the spinel-type  $\text{Li}_4\text{Ti}_5\text{O}_{12}$  (JCPDS Card No. 49-0207), with the space group  $Fd-3m$  spinel. Meanwhile, the refined lattice parameter of  $\text{Li}_4\text{Ti}_5\text{O}_{12}$ , which is consistent with results reported by Ohzuku et al [3].

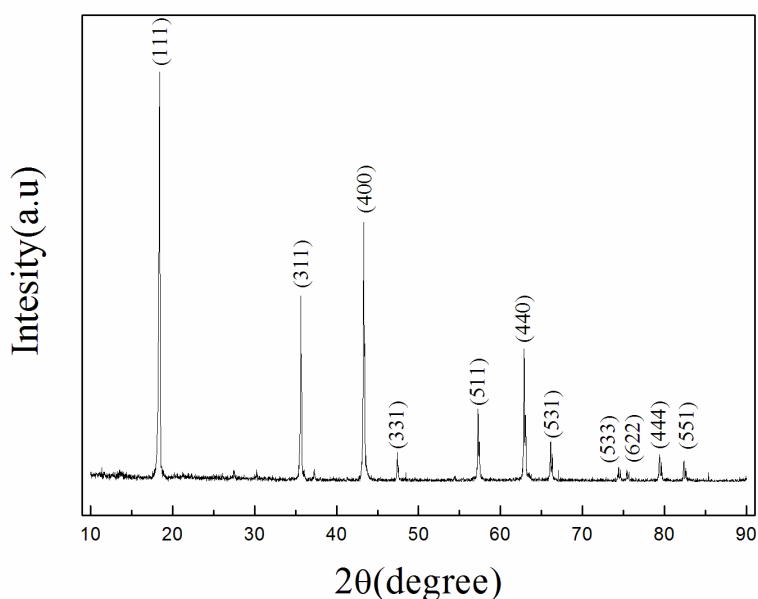


**Figure 1.** XRD diffraction patterns of nano- $\text{Li}_4\text{Ti}_5\text{O}_{12}$  samples.

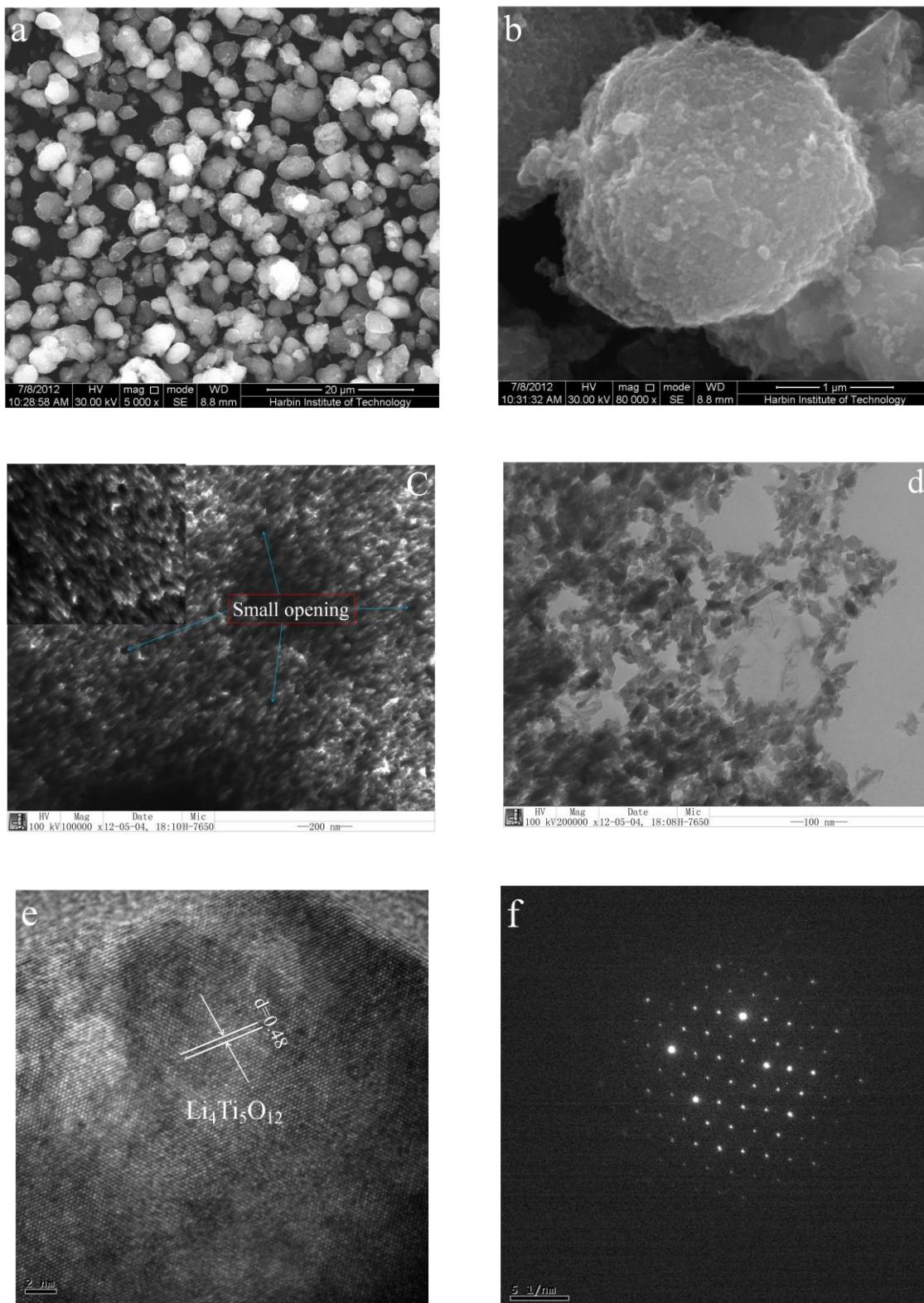


**Figure 2.** (a) and (b) Representative SEM image, (c) and (d) TEM image, (e) and (f) HRTEM image of the nano- $\text{Li}_4\text{Ti}_5\text{O}_{12}$ .

Fig. 2a shows the morphology of the  $\text{Li}_4\text{Ti}_5\text{O}_{12}$ , which are well ordered and relatively uniform microspheres with average diameter of 1.5-2  $\mu\text{m}$  (Fig. 2b). To further examine the architecture of the  $\text{Li}_4\text{Ti}_5\text{O}_{12}$  microspheres, the samples were investigated by TEM, as shown in Fig. 2c. It can be seen

that clavate particle is upright and orderly distributed in the surface of the microspheres. Meanwhile, many pores, about 20 nm poresize, are found between particles, this unique morphology would make the active material contact with electrolyte more sufficiently, leading to improve electrochemical property. Upon magnifying to higher resolution (Fig. 2d), the particle displayed large scale nano-particle of size 30–40 nm. It is expected that such a structure plays a vital role in enhancing the rate performance via reducing the diffusion path length for ionic and electronic mobility. The high resolution electron microscopy (Fig. 2e) further reveals that the crystalline region with clear lattice fringes has an inter-planar spacing of 0.48 nm, consistent with the (111) atomic planes of the spinel structure, indicating that the well-crystallized spinel phase in the nanostructured materials was prepared. Fig. 2f is an electron diffraction pattern collected from the same sample [36-38]. Calculated lattice spacings are in agreement with JCPDS reference card no. 49-0207 for cubic  $\text{Li}_4\text{Ti}_5\text{O}_{12}$ , and the FFT pattern also confirms the formation of a highly crystallized spinel phase. Fig.3 shows the constant current initial charge–discharge curves of the nano- $\text{Li}_4\text{Ti}_5\text{O}_{12}$  pore microspheres at different rates from 1 to 60 C between 1.0 and 2.5V.  $\text{Li}_4\text{Ti}_5\text{O}_{12}$  show outstanding rate performance. At the initial rate of 1 C, the potential plateau can be seen at around 1.55 V with a discharge capacity of  $168.3 \text{ mAh g}^{-1}$ . It should be pointed out that the high coulombic efficiency (ca. 99.3%) in the first cycle might be ascribed to the perfect crystallization degree and nano-particle size, which decrease the irreversible capacity. The reversible capacity decreases to 157, 143, 133, 123, 108, 91 and 80  $\text{mAh g}^{-1}$  when the density rate increases to 3 C, 5 C, 10 C, 20 C, 30 C, 40 C and 60 C, respectively. Although the capacity and the potential plateau both decrease with increasing current density, a high capacity of  $80 \text{ mAh g}^{-1}$  is still maintained even at 60 C. The significant improvement in the rate performance can be mainly attributed to good crystallinity and the short lithium diffusion path [28,39].

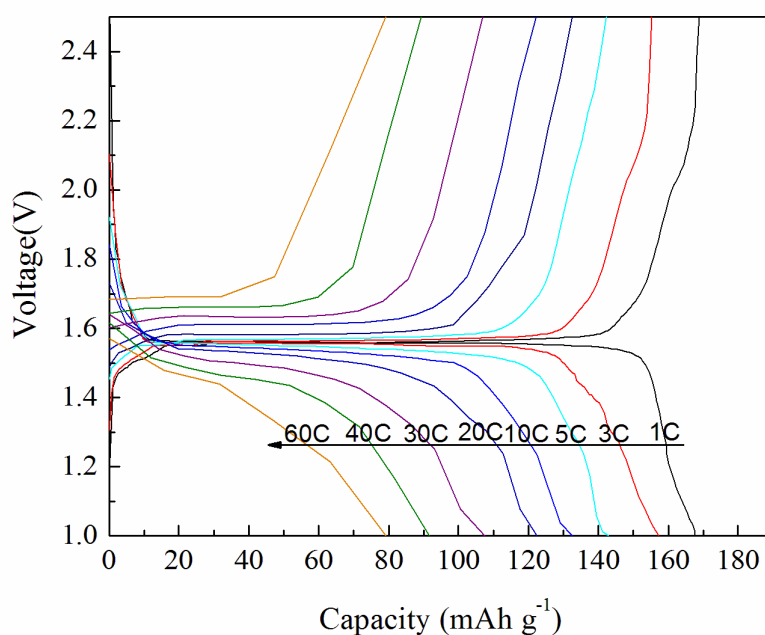


**Figure 3.** Charge-discharge curves for nano- $\text{Li}_4\text{Ti}_5\text{O}_{12}$  between 1.0 and 2.5V at different current densities.

Fig. 4 shows the rate and cycle performances of nano- $\text{Li}_4\text{Ti}_5\text{O}_{12}$  pore microspheres. For each stage, the process was taken with 50 cycles. As shown in Fig. 4, an excellent cycling performance is observed for  $\text{Li}_4\text{Ti}_5\text{O}_{12}$  electrode, even at the higher rate of 60C. The capacity loss is only in the range of 0.01-0.02% within per 50 cycles at all current rates, indicating the high stability of the as-derived  $\text{Li}_4\text{Ti}_5\text{O}_{12}$  in repeated cycles. In addition, the coulombic efficiency stayed at about 100%, demonstrating an excellent cycling performance of  $\text{Li}_4\text{Ti}_5\text{O}_{12}$ . The high-rate charge-discharge capability of  $\text{Li}_4\text{Ti}_5\text{O}_{12}$  could mainly be deduced from facile  $\text{Li}^+$  ion diffusion in the nanocrystal structures [32, 33, 40].

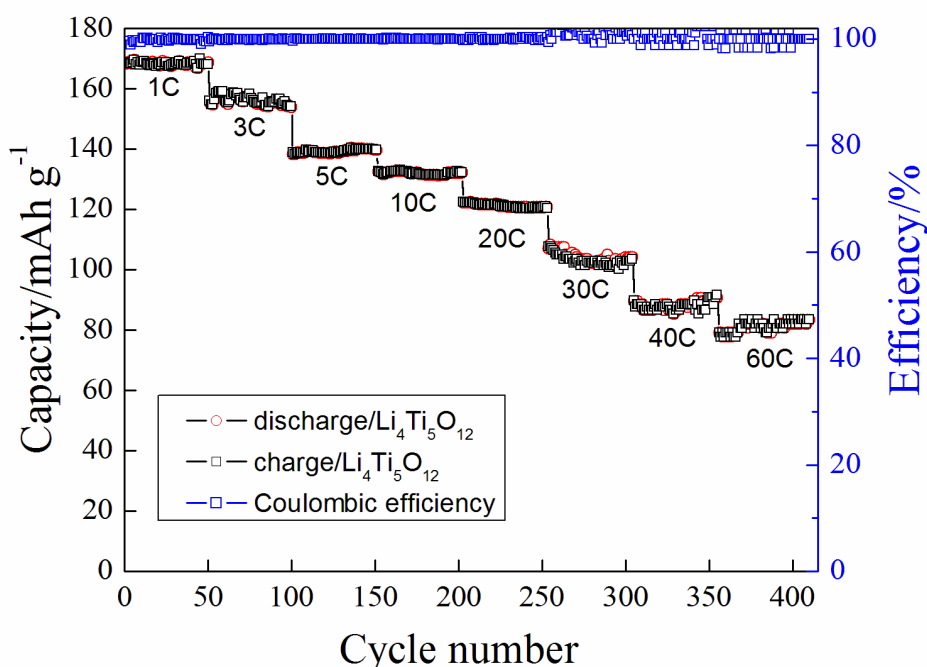


**Figure 4.** Plots of charge-discharge capacity versus cycle number and coulombic efficiency versus cycle number under different current rates.

#### 4. CONCLUSION

In conclusion, the nano- $\text{Li}_4\text{Ti}_5\text{O}_{12}$  pore microspheres were synthesized by hydrothermal and short time calcination method. The prepared  $\text{Li}_4\text{Ti}_5\text{O}_{12}$  presents the morphology of pore microspheres structure, which would guarantee sufficient contact between active material and electrolyte, particle size is ranging between 20–50 nm, thus facilitating the electrochemical storing Li. At rate of 1 C is achieved a capacity value of 168.3 mAh g<sup>-1</sup>, capacity value close to the theoretical value of 175 mAh g<sup>-1</sup>. In addition, in lithium batteries at high-rate, the polarization remains small, and high lithium ion insertion, the nano- $\text{Li}_4\text{Ti}_5\text{O}_{12}$  pore microspheres demonstrated superior rate capability even at a 10 C rate retained over 93% capacity of 1C. Irrespective of rates used,  $\text{Li}_4\text{Ti}_5\text{O}_{12}$  retain their initial capacity up to 50 cycles. These results suggest that nano- $\text{Li}_4\text{Ti}_5\text{O}_{12}$  pore microspheres is superior in terms of

both high rate-capability and capacity retention is ascribed to nano and pore structure of the electrodes that provide more short and faster diffusion-paths for Li .

#### ACKNOWLEDGEMENTS

This work is funded by Special Foundation for Harbin Talents Scientific and Technological Innovation of China (No. 2009RFQXG047), Natural Science Foundation of China (No. 50902038) and Education Department of Jilin Province (No. 2010216).

#### References

1. S. Scharner, W. Weppner and P. Schmid-Beurmann, *J. Electrochem. Soc.*, 146 (1999) 857.
2. L. Aldon, P. Kubiak, M. C. Womes, J. Jumas, J. Olivier-Fourcade, J. L. Tirado, J. I. Corredor and C. P. Vicente, *Chem. Mater*, 16 (2004) 5721.
3. T. Ohzuku, A. Ueda, N. Yamamoto, *J. Electrochem. Soc.*, 142 (1995) 1431.
4. M. M. Thackeray, *J. Electrochem. Soc.*, 142 (1995) 2558.
5. K. Zaghib, M. Simoneau, M. Armand and M. Gauthier, *J. Power Sources*, 81 (1999) 300.
6. D. Permunage and K. M. Abraham, *J. Electrochem. Soc.*, 145 (1998) 2609.
7. G. G. Amatucci, F. Badway, A. D. Pasquier and T. Zheng, *J. Electrochem. Soc.*, 148 (2001) A930.
8. D. Mikhailova, A. Sarapulova, A. Voss, A. Thomas, S. Oswald, W. Gruner, D. M. Trots, N. N. Bramnik and H. C. Ehrenberg, *Mater*, 22 (2010) 3165.
9. C. Y. Ouyang, Z. Y. Zhong, M. S. Lei, *Electrochem. Commun.* 9 (2007) 1107.
10. Z. Yang, D. Choi, S. Kerisit, K. M. Rosso, D. Wang, J. Zhang, G. Graff, J. J. Liu, *J. Power Sources*, 192 (2009) 588.
11. E. Kang, Y. S. Jung, G. H. Kim, J. Y. Chun, U. Wiesner, A. C. Dillon, J. K. Kim and J. Lee, *Adv. Funct. Mater.*, 21 (2011) 4349.
12. K. N. Jung, S. Pyun and S. W. Kim, *J. Power Sources*, 637 (2003) 119.
13. H. G. Jung, S. T. Myung, C. S. Yoon, S. B. Son, K. H. Oh, K. Amine, B. Scrosati and Y.-K. Sun, *Energy Environ. Sci.*, 4 (2011) 1345.
14. R. Cai, X. Yu, X. Q. Liu and Z. P. Shao, *J. Power Sources*, 195, (2010) 8244.
15. S. H. Huang, Z. Y. Wen, B. Lin, J. D. Han and X. G. Xu, *J. Alloys. Compounds*, 457 (2008) 400.
16. C. H. Chen, J. T. Vaughey, A. N. Jansen, D. W. Dees, A. J. Kahaian, T. Goacher and M. M. Thackeray, *J. Electrochem. Soc.*, 148 (2001) A102.
17. S. Z. Ji, J. Y. Zhang, W. W. Wang, Y. Huang, Z. R. Feng, Z. T. Zhang and Z. L. Tang, *Materials Chemistry and Physics.*, 123 (2010) 510.
18. H. Zhao, Y. Li, Z. Zhu, J. Lin, Z. Tian, R. Wang, *Electrochim. Acta*, 53 (2008) 7079.
19. L. Cheng, J. Yan, G. N. Zhu, J. Y. Luo, C. X. Wang and Y. Y. Xia, *J. Mater. Chem.*, 20 (2010) 595.
20. K. S. Park, A. Benayad, D. J. Kang, S. G. Doo, *J. Am. Chem. Soc.*, 130 (2008) 14930.
21. L. Zhao, Y. S. Hu, H. Li, Z. X. Wang and L. Q. Chen *Adv. Mater.*, 23, (2011) 1385.
22. K. Naoi, S. Ishimoto, Y. Isobe and S. Aoyagi, *J. Power Sources*, 195 (2010) 6250.
23. X. Li, M. Z. Qu, Y. J. Huai and Z. L. Yu, *Electrochimica. Acta*, 55 (2010) 2978.
24. Y. Shi, L. Wen, F. Li and H. M. Cheng, *J. Power Sources*, 196 (2011) 8610.
25. D. H. Kim, Y. S. Ahn and J. Kim, *Electrochem. Commun.*, 7 (2005) 1340.
26. E. M. Sorensen, S. J. Barry, H. K. Jung, J. R. Rondinelli, J. T. Vaughey and K. R. Poeppelmeier, *Chem. Mater.*, 18 (2006) 482.
27. L. Kavan and M. Gratzel, *Electrochem. Solid State Lett.*, 5 (2002) A39.
28. C. Jiang, M. Ichihara, I. Honma and H. S. Zhou, *Electrochim. Acta*, 52 (2007) 6470.
29. J. R. Li, Z. L. Tang and Z. T. Zhang, *Electrochem. Commun.*, 7 (2005) 894.
30. L. C. Yang, Q. S. Gao, Y. H. Zhang, Y. Tang and Y. P. Wu, *Electrochem. Commun.*, 10 (2008)

118.

31. J. Haetge, P. Hartmann, K. Brezesinski, J. Janek and T. Brezesinski, *Chem. Mater*, 23 (2011) 4384.
32. J. Z. Chen, L. Yang, S. H. Fang and Y. F. Tang, *Electrochimica. Acta*, 55 (2010) 6596.
33. Z. S. Hong, X. Z. Zheng, X. K. Ding, L. L. Jiang, M. D. Wei and K. M. Wei, *Energy Environ. Sci*, 4 (2011) 1886.
34. H. G. Jung, S. W. Oh, J. Ce, N. Jayaprakash and Y. K. Sun, *Electrochem. Commun*, 11 (2009) 756.
35. Y. F. Tang, L. Yang, Z. Qiu and J. S. Huang, *J. Mater. Chem.*, 19 (2009) 5980.
36. S. H. Yu, A. Pucci, T. Hertrich, M. G. Willinger, S. H. Baek, Y. E. Sung and Nicola Pinna, *J. Mater. Chem.*, 21 (2011) 806.
37. A. S. Prakash, P. Manikandan, K. Ramesha, M. Sathiya, J.-M. Tarascon, and A. K. Shukla, *Chem. Mater.*, 22 (2010) 2857.
38. Y. F. Tang, L. Yang, Z. Qiu and J. S. Huang, *Electrochem. Commun*, 10 (2008) 1513.
39. P. G. Bruce, B. Scrosati, J.-M. Tarascon and Angew, *Chem. Int. Ed*, 47 (2008) 2930.
40. L. F. Shen, X. G. Zhang, E. Uchaker, C. Z. Yuan and G. Z. Cao, *Adv. Energy Mater*, 2 (2012) 691.